HYPERSPECTRAL REMOTE SENSING WITH THE UAS "STUTTGARTER ADLER" - CHALLENGES, EXPERIENCES AND FIRST RESULTS

A. Buettner[a,*], H. P. Roeser[a]

[a] Institute of Space Systems, University of Stuttgart, 70569 Stuttgart, Germany -
(buettner, roeser) @irs.uni-stuttgart.de

KEY WORDS: Hyperspectral, Remote Sensing, Unmanned Aerial System, Precision Agriculture, Direct Georeferencing, Calibration

ABSTRACT:

The UAS "Stuttgarter Adler" was designed as a flexible and cost-effective remote-sensing platform for acquisition of high quality environmental data. Different missions for precision agriculture applications and BRDF-research have been successfully performed with a multispectral camera system and a spectrometer as main payloads. Currently, an imaging spectrometer is integrated in the UAS as a new payload, which enables the recording of hyperspectral data in more than 200 spectral bands in the visible and near infrared spectrum. The recording principle of the hyperspectral instrument is based on a line scanner. Each line is stored as a matrix image with spectral information in one axis and spatial information in the other axis of the image. Besides a detailed specification of the system concept and instrument design, the calibration procedure of the hyperspectral sensor system is discussed and results of the laboratory calibration are presented. The complete processing chain of measurement data is described and first results of measurement-flights over agricultural test sites are presented.

1 INTRODUCTION

Hyperspectral remote sensing data is of great interest in many different research topics and applications. It combines traditional 2D imaging remote sensing technology with classical spectroscopy and allows the acquisition of data with both, geometric and spectral high resolution. The large number of spectral bands provides the ability to derive biophysical and biochemical parameters from the quasi continuous visible and near infra-red spectrum (Haboudane et al., 2008), while the geometric resolution can be used for the creation of rectified image stripes. In the last decades, hyperspectral remote sensing was mainly performed with airborne sensors such as AVIRIS or HyMap, which are flown on manned aircraft (Green et al., 1998, Cocks et al., 1998). The development of compact and lightweight imaging spectrometers in the last few years offers the possibility to integrate such instruments in small unmanned aerial systems (UAS) and closes the gap between time-consuming and spatially limited point measurements on the ground and complex and expensive flight campaigns with manned aircraft. The UAS "Stuttgarter Adler" is operated as a remote sensing platform at the Institute of Space Systems and can be equipped with different sensor systems like multispectral and thermal cameras (Kirchgaessner, 2012). The integration of an imaging spectrometer as hyperspectral payload extends the range of applications, but also comes along with lots of new challenges.

2 SYSTEM OVERVIEW

2.1 UAS "Stuttgarter Adler"

The UAS Stuttgarter Adler is a remote sensing platform, which was specially designed for acquiring high quality remote sensing data with great flexibility at comparatively low costs (Putze, 2012). The twin-engine configuration with two 2.0 kW electrical engines allows a take-off weight of 25 kg including a payload capacity of 4-5 kg, the wingspan adds up to 4.33 m. The aerodynamic design accounts for stable flight at 12 - 15 m/s airspeed. Radio link and all control surfaces are constructed in redundant way so that no single point failure leads to loss of the aircraft. The integration of the motors in two nacelles provides enough

space for the integration of the payload in the fuselage. Take off and landing require a paved or grass runway of 150 m length and are performed manually with remote control, the measurement flight itself is controlled completely autonomous by an autopilot system based on the open source project "paparazzi" (Brisset, 2006). The LiPo batteries allow a total flight-time of up to 30 minutes, technical data of the UAV can be found in Fig.1.

Figure 1: UAS "Stuttgarter Adler" before take-off

Wing span	4.33 m
Length	2.6 m
Max. TOW	25 kg
Electrical propulsion	2×2 kW
Batteries	$2 \times$ 10s2p 8000 mAh LiPo
Payload capacity	4 – 5 kg
Flight time	25 – 30 min

Table 1: Technical data of the UAV

2.2 Hyperspectral Sensor System

The hyperspectral imager consists of three main components, see Fig. 2 (Spectral Imaging Ltd., 2008). Incoming light is focused

on the entrance-slit of the spectrograph by a special fore-lens (OLE9 FORE LENS); a monochrome CCD-camera (PROSIL-ICA GE1900) is mounted on the back of the spectrograph to detect the radiance; the spectrograph itself (SPECIM IMSPECTOR V10E) disperses the light and focuses it on the CCD detector surface with a spectral resolution of 2.8 nm. The specification of the instrument is shown in Tab. 2.
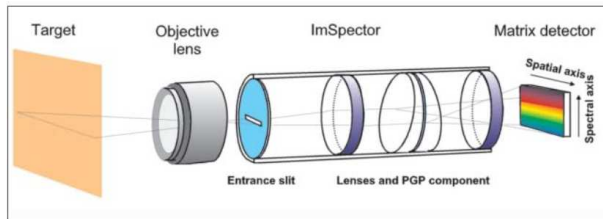

Figure 2: Schematic of the imaging spectrograph

Spectrograph	
Spectral range	380 – 1100 nm
Spectral resolution	2.8 nm
Numerical aperture	F / 2.4
Slit width	30 μm
Spatial resolution	rms spot radius $< 9\,\mu$m
CCD camera and forelens	
Resolution	1920 $\times$ 1080 pixel
Binning h/v	1 - 8 pixel / rows
Pixel size	7.4 $\times$ 7.4 μm
Radiometric resolution	12 bit
Frame rate	up to 30 fps (full resolution)
Focal length	9 mm
Field of view	76.5$°$ $\times$0.19$°$

Table 2: Specification of the hyperspectral imager

The hyperspectral imager is working as a push broom line scanner, with the entrance slit oriented perpendicular to the flight direction. The constant movement of the UAV is used to scan an area in continuous stripes. Each single line is stored as a matrix image, which contains spectral information in one dimension and spatial information in the other dimension of the image sensor. The geometric rectification of the image stripes is a big challenge in operating a line scanner in an UAV. The small platform is susceptible to gusts of wind and much more unstable in comparison to large manned aircraft. For correct alignment and rectification of the recorded lines, the position and attitude of the sensor must be known with high precision. Therefore, additional sensors for position and attitude determination are mounted on the spectrograph. The position and attitude sensor system comprises three-axis MEMS accelerometer, gyroscope and magnetometer, a L1-GPS receiver providing raw measurement data and a barometer and thermometer as additional sensors for improving the height determination. The gyroscope used is an ITG-3200 triple-axes gyroscope from Invensense providing three integrated 16-bit ADCs for simultaneous sampling of the gyros. The accelerometer is an Analog Devices ADXL345 digital triaxial acceleration sensor with measurement range up to 16 g, which was designed for low power consumer market. The 13-bit resoultion enables measurement of inclination changes smaller than 0.5$°$. The Honeywell HMC5883L triple-axes sensor is used as digital compass in the hardware setup. The 12-bit ADC enables measurements with milligauss resolution, which lead to a heading accuracy of 1 - 2$°$. An external professional grade GNSS-antenna from Tallysman is used for acquiring strong GPS signal and im-

proved multipath rejection. The inertial data is recorded with 100 Hz, while the GPS receiver provides raw data with 20 Hz update rate. A small microprocessor board is used for synchronous sensor readout via fast-mode i2c digital interface, a precise GPS pulse-per-second time-signal serves as common time basis. Since no real-time capability is required, a specially designed Extended Kalman Filter with smoothing techniques is used for sensor fusion of IMU and GPS data in the post-processing (Koerner, 2012). The information flow of the filter is shown in Fig. 3. The whole
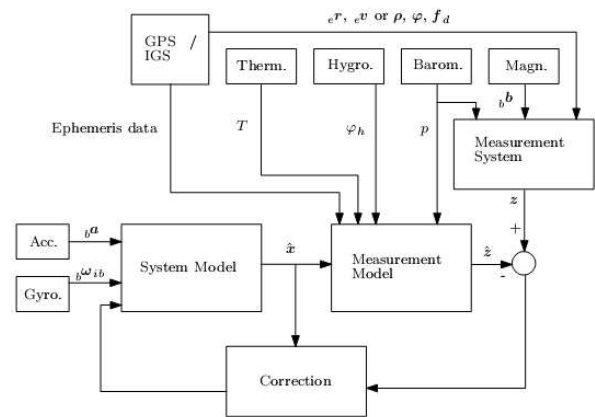

Figure 3: Information flow of the extended Kalman filter

sensor system is fixed horizontally on a common mounting plate. An optical mirror reflects the incoming light to the forelens. EPP-foam is used for vibration isolation from the aircraft. The IMU is mounted directly on top of the spectrometer to keep the position and orientation offset as constant and small as possible. The GPS-antenna is mounted on top of the aircraft right above the instrument for best reception of the GPS satellite signals. A compact PC with Linux operating system, Gigabit-Ethernet interface and solid-state disk for data storage is used as on-board payload computer. Custom software for configuration of the camera and recording of the image data was developed, which enables flexible adjustments of different sensor parameters such as frame rate, binning, and exposure time for particular missions.

3 CALIBRATION AND CHARACTERIZATION

Radiometric and spectral calibration is performed in house in an optical laboratory. Different calibration equipment such as an integrating sphere, line emission lamps and a monochromator are available for regular calibration in the laboratory between measurement campaigns. The whole system including mounting plate and mirror is calibrated together to account for possible distortions of the additional components.

3.1 Radiometric Calibration

The main task of radiometric calibration is the determination of the coefficients for the conversion of raw data (DN) into physical units (spectral radiance, mW / m^2 sr nm). In addition, vignetting effects and sensor inhomogeneities due to slightly varying sensitivities of the CCD elements are corrected. An integrating sphere, which is regularly calibrated against German national standard (PTB), is used as homogeneous light-source with known spectral radiance. The calibration is valid for the spectral range from 380 nm to 1100 nm with a relative uncertainty of ± 5 %. For the determination of the sensor linearity, the integrating sphere is equipped with a adjustable slit in front of the QTH lamp and an optometer for measuring the total radiance. The linearity of the radiometric response function is measured by increasing the

luminosity up to saturation level at different integration times. Dark signal is quantified in the laboratory for different temperatures and integration times to characterize the dark signal non uniformity (DSNU). Noise equivalent spectral radiance (NESR) is determined by measuring the standard deviation of the dark signal and can be used for signal-to-noise-ratio (SNR) analysis. The radiometric calibration coefficient for the nadir pixel is shown in Fig. 4, the according NESR for an integration time of 1 ms is shown in Fig. 5. The spectral region above 1000 nm is strongly influenced by system noise due to the low quantum efficiency of the CCD-Sensor in this region and therefore discarded in further data analysis.
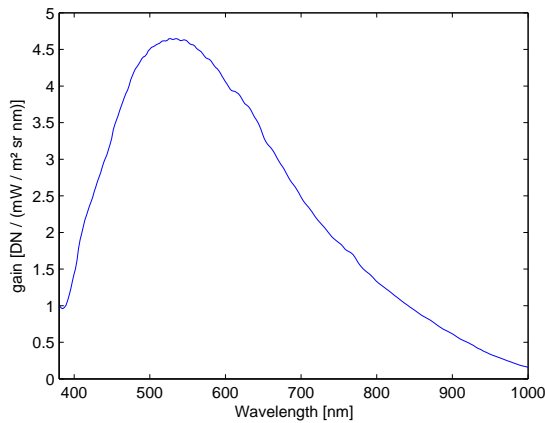

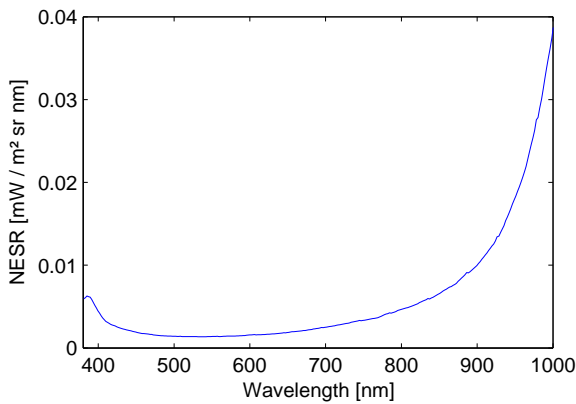Figure 4: Radiometric calibration coefficient

Figure 5: Noise equivalent spectral radiance for 1 ms integration time

3.2 Spectral Calibration

Spectral calibration is needed to successfully determine reflectance spectra or physical parameters of measurement targets. It describes the response of the sensor to discrete light and is used to determine the centre wavelengths and spectral resolution for each spectral channel. The response function of each channel can be approximated with a Gaussian shaped curve, the spectral resolution is defined as the full width half maximum (FWHM) of the function. The peak response of the spectrometer to an infinitesimally narrow emission line describes the centre wavelength of each channel. Special line emission lamps with different gas fills are used to produce narrow, intense lines from the excitation of the gases. Measurements with HgAr–, Xe– and Ne–gas lamps provide emission lines, which cover the whole spectral range. The line width of the emission lines is much smaller than

the spectral resolution of the spectrograph and thus well suited for wavelength calibration (Chen, 1997). Figure 6 shows the response of the nadir channels to the Xenon lines, in Fig. 7 the 4 th order polynomial-fit for the wavelength calibration of the spectral channels is shown. The nominal spectral resolution of the spectrograph is stated as 2.8 nm by the manufacturer. Results of measurements with line emission lamps and monochromator showed a FWHM between 3.2 nm an 4.7 nm, depending on the spectral channel. The 1080 spectral pixels of the CCD-Sensor are binned with the factor of 3 which leads to 331 spectral channels in the 380 - 1100 nm region with a spectral sampling interval of approximately 2.2 nm. Thus, the binning reduces the data volume and increases the SNR without loosing spectral information.
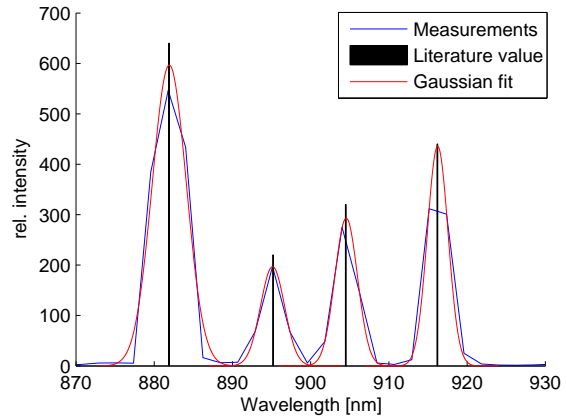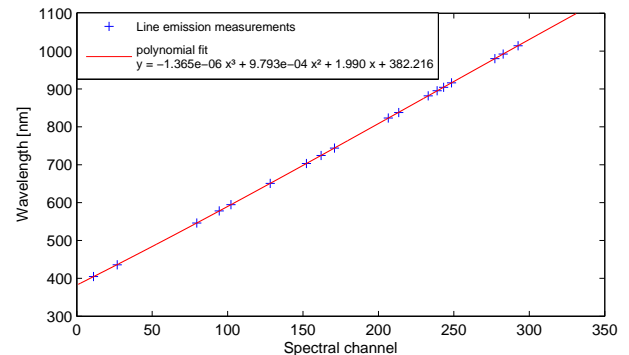

Figure 6: Measurement of Xenon lines

Figure 7: Wavelength calibration with line emission lamps

4 RESULTS AND DISCUSSION

4.1 Data processing

The results of the laboratory calibration are used for radiometric pre-processing after measurement flights. In a first step, the raw data is corrected for dark signal and can then be converted to spectral radiance by applying the radiometric calibration coefficients. Afterwards, atmospheric distortions have to be corrected. This can be done using radiative transfer tools based on the open source software package libRadtran. Besides time, date and location, further input-parameters like temperature and humidity are measured during flight time. In addition, a sun-photometer is used to measure the aerosol-optical depth. As an alternative method, the reflected radiance of a calibrated diffuse grey reference panel with 50 % reflectance level can be measured before and after a flight. Reference values are calculated through linear

interpolation for the whole flight to derive reflectance values. Finally, geometric rectification and georeferencing have to be performed. Position and attitude of the aircraft is calculated in post-processing with 100 Hz. The beginning and end of each image stripe is triggered by the autopilot and marked with a GPS timestamp. A camera-timestamp is stored in every single line-image and used for connecting the images with the position and attitude of the UAS at each exposure. Based on the collinear equations, custom software was developed for direct georeferencing of the image stripes in UTM coordinates on flat terrain or digital elevation model. The correction of boresight angles is implemented with a differential rotation matrix. Final data is stored in ENVI-compatible format and can be further processed with classical remote sensing software packets.

4.2 First flight tests and measurement flights

In early 2012, first flight tests were performed to prove the system under operational conditions. Parameters like frame rate, exposure time and flight speed were adapted to avoid gaps in image stripes. IMU and GPS measurements of the test flights were used for tuning of the Kalman-filter. In summer 2012, first measurement flights over agricultural test fields were performed. The flight altitude was 300 m above ground. A framerate of 20 fps and an average speed of 15 m/s lead to a ground sampling distance of 0.5×1 m. The data was spatially resampled with nearest neighbour method to match a 1×1 m UTM grid. Figure 8 shows an openstreetmap aerial photo which is overlayed with a part of an hyperspectral image-stripe in RGB-representation. The hyperspectral image section covers different areas like forest, bare soil or asphalt. Three pre-processed reflectance spectra, which were directly extracted from single pixels of the image in Fig. 8, are shown in Fig. 9. The vegetation reflectance spectrum differs clearly from the other reflectance spectra and shows the typical maximum in the green wavelength along with the significant red edge transition zone between visible and near infrared wavelength. These features provide the basis for further investigations like estimation of chlorophyll content, leaf area index or other biophysical parameters (Liu et al., 2004). Also, heterogeneities within one agricultural field are visible and can be utilized for estimating yields or variable-rate application of nitrogen.

5 CONCLUSION AND FUTURE WORK

The hyperspectral sensor system was chosen as a new payload to enable the recording of high spectral resolution imagery in the visible and near infrared spectrum, with high temporal flexibility at low operational costs. The system could be successfully integrated in the remote sensing platform "Stuttgarter Adler" and showed the ability to generate detailed remote sensing data, which is useful for various applications in the field of precision farming. Based on calibration methods in the laboratory and reference field measurements, a complete processing chain was developed to generate a radiometric and spectral calibrated image. Photogrammetric methods were applied for direct georeferencing of the image stripes. First results show, that there are still geometric distortions which are not corrected properly. S-shaped errors, which are visible on straight lines like the street in Fig. 8, may result from limited accuracy of the MEMS-sensors. Further adaptions of the Kalman-Filter shall be investigated to minimize these errors. For absolute accuracy assessment, measurements with ground control points and an additional matrix-camera, which is triggered parallel to the line scanner with the same frequency, shall be performed this summer.
In cooperation with the Institute of Crop Science of the University of Hohenheim, hyperspectral remote sensing data shall be

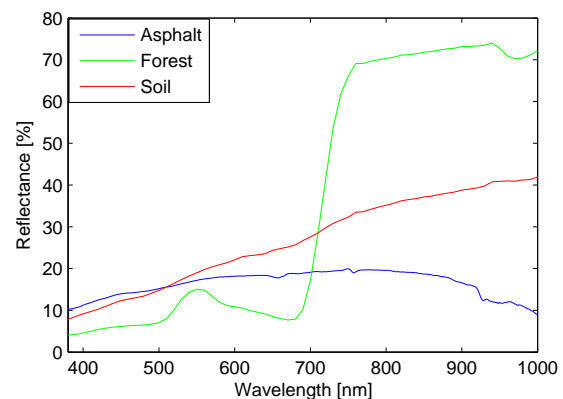Figure 8: Image stripe in RGB-representation; map: © OpenStreetMap

Figure 9: Reflectance spectra for asphalt, forest and soil

used for the determination of spectral characteristics of winter wheat and compared with ground based measurements during the vegetation period 2013.

REFERENCES

Brisset, P., 2006. The Paparazzi solution. In: Micro Air Vehicle Conference 2006. See also URL www.recherche.enac.fr/paparazzi/papers_2006/mav06_paparazzi.pdf.

Chen, H., 1997. Remote sensing calibration systems: an introduction. Studies on geophysical optics and remote sensing, A. Deepak.

Cocks, T., Jenssen, R., Stewart, A., Wilson, I. and Shields, T., 1998. The hymap airborne hyperspectral sensor: the system, calibration and performance. In: 1st EARSeL workshop on imaging spectrometry, pp. 37–42.

Green, R. O., Eastwood, M. L., Sarture, C. M., Chrien, T. G., Aronsson, M., Chippendale, B. J., Faust, J. A., Pavri, B. E., Chovit, C. J., Solis, M., Olah, M. R. and Williams, O., 1998. Imaging spectroscopy and the airborne visible/infrared imaging spectrometer (aviris). Remote Sensing of Environment 65(3), pp. 227 – 248.

Haboudane, D., Tremblay, N., Miller, J. and Vigneault, P., 2008. Remote estimation of crop chlorophyll content using spectral indices derived from hyperspectral data. Geoscience and Remote Sensing, IEEE Transactions on 46(2), pp. 423–437.

Kirchgaessner, U., 2012. Einsatz eines ferngesteuerten Kleinflugzeugs zur Erfassung von Umweltdaten. Dissertation, University of Stuttgart.

Koerner, F., 2012. Design of a Kalman Filter for Tightly Coupled GPS/INS Integration. Diploma-thesis, University of Stuttgart.

Liu, J., Miller, J., Haboudane, D. and Pattey, E., 2004. Exploring the relationship between red edge parameters and crop variables for precision agriculture. In: Geoscience and Remote Sensing Symposium, 2004. IGARSS '04. Proceedings. 2004 IEEE International, Vol. 2, pp. 1276–1279.

Putze, U., 2012. Auslegung und Instrumentierung eines ferngesteuerten Kleinflugzeuges fuer die Erdbeobachtung. Dissertation, University of Stuttgart.

Spectral Imaging Ltd., 2008. ImSpector imaging spectrograph user manual.